

## Crystallization kinetics in the system $\text{CaMgSi}_2\text{O}_6$ - $\text{CaAl}_2\text{Si}_2\text{O}_8$ : development of zoning and kinetics effects on element partitioning

AKIRA TSUCHIYAMA<sup>1</sup>

Geological Institute, University of Tokyo, Hongo, Tokyo, 113 Japan

### Abstract

Compositional zoning of Al in diopside phenocrysts and Mg in anorthite phenocrysts grown from melts of the system  $\text{CaMgSi}_2\text{O}_6$ - $\text{CaAl}_2\text{Si}_2\text{O}_8$  has been investigated. Reverse zoning in which Al in diopside or Mg in anorthite decreases from core to rim is produced in the isothermal crystallization experiments, whereas normal zoning is produced in the continuous cooling experiments. In the isothermal crystallization experiments, Al content at the diopside rim decreases with increasing time and then becomes a constant value, which corresponds to the equilibrium composition. Melt composition near the diopside-melt interface also deviates from the equilibrium value during growth. The partition coefficient between the core of the crystal and the starting liquid increases with increasing supercooling. It is concluded from these results that interface equilibrium is not maintained at the beginning of growth of the crystals, but the interface kinetics by which excess amounts of solute (Al or Mg) are incorporated into the crystals during growth ("solute trapping") plays a significant role in the formation of reverse zoning. Reverse zoning is formed by the process in which the crystal grows fast with initial large supercooling and finally ceases to grow in equilibrium with the residual liquid at a constant temperature. In the continuous cooling experiments, it is proposed that normal zoning can be produced even if the interface kinetics is significant. The partition coefficient between the core of the crystal and the starting liquid is scattered even at the same cooling rate but has a tendency to increase with increasing cooling rate. The partition coefficient for diopside is correlated with its morphology. This correlation suggests that the composition of the core is determined by the supercooling at the time of the nucleation of crystals in the cooling liquid.

### Introduction

In order to understand chemical zoning in minerals, it has been generally assumed that equilibrium is maintained at the crystal-liquid interface during growth of the crystals (e.g., Smith, 1974; Albarede and Bottinga, 1972). There is no reason, however, to assume interface equilibrium *a priori* (Dowty, 1980). In fact, disequilibrium at the interface is observed experimentally in the growth of crystals from aqueous solutions (e.g., Kern, 1953). Theoretical treatments of growth mechanisms, in which reactions at the interface (interface kinetics) are taken into consideration, exist for various industrial systems (e.g., Burke, 1965; Brice, 1973). Furthermore, the compositions of crystals by interface kinetics were discussed in a binary system (Baker and Cahn, 1971; Hopper and Uhlmann, 1974; Dowty, 1980).

Various kinds of zoning in minerals have been formed in dynamic crystallization experiments during the last decade (e.g., Lofgren, 1974; Donaldson et al., 1975; Usselman et al., 1975; Walker et al., 1976; Bianco and Taylor, 1977; Grove and Bence, 1977, 1979; Gamble and Taylor, 1980; Lofgren, 1980). Some of them can be explained by assuming interface equilibrium during growth of minerals

(e.g., Donaldson et al., 1975; Walker et al., 1976; Bianco and Taylor, 1977; Lofgren, 1980). However, there are some results which suggest the importance of interface kinetics, such as the formation of reverse zoning in plagioclase at a constant temperature (Lofgren, 1974), mineral/liquid partition coefficients of some elements affected by the cooling rate (e.g., Grove and Bence, 1977, 1979; Gamble and Taylor, 1980; Lofgren, 1980; Kirkpatrick et al., 1981), and heterogeneous melt composition around olivine crystals (Kirkpatrick et al., 1981). Kouchi et al. (1983a,b) measured the growth rates of olivine and pyroxene and their partition coefficients, and concluded that interface kinetics were important. Sector zoning in minerals is also suggestive of an important role of interface kinetics during growth of minerals (e.g., Nakamura, 1973; Dowty, 1976, 1980; Kitamura and Sunagawa, 1977; Kouchi, 1983b).

Little knowledge of the details of interface kinetics in silicate systems is presently available, mainly because many silicate systems used in the previous dynamic crystallization experiments are compositionally too complex to interpret. In this paper, the zoning of Al in diopside and Mg in anorthite and the kinetics of element partitioning between the crystals and liquid during growth are investigated. The crystals were produced as phenocrysts as a function of time and degree of supercooling or cooling rate in

<sup>1</sup> Present Address: Department of Geology, University of Oregon, Eugene, OR 97403, U.S.A.

the dynamic crystallization experiments on the system  $\text{CaMgSi}_2\text{O}_6\text{-CaAl}_2\text{Si}_2\text{O}_8$  (Tsuchiyama, 1983). This system is treated as a type of binary system, and interface kinetics and the development of the zoning are discussed in detail in terms of the previous theory in a binary system. The attainment of equilibrium in "equilibrium" runs, and relation between the composition and morphology of the diopside phenocrysts are also discussed.

### Experimental technique

Experiments were carried out with three different starting materials of synthetic glasses ( $\text{Di}_{80}:\text{Di}_{81.1}\text{An}_{18.9}$  with diopside liquidus at  $1330^\circ\text{C}$ ;  $\text{Di}_{64}:\text{Di}_{64.2}\text{An}_{35.8}$  near the diopside-anorthite eutectic at  $1270^\circ\text{C}$ ;  $\text{Di}_{50}:\text{Di}_{49.2}\text{An}_{50.8}$  with anorthite liquidus at  $1360^\circ\text{C}$ ). The Pt-wire loop method was used except for some runs with  $\text{Di}_{80}$  in which  $\text{Pt}_{90}\text{Au}_{10}$  capsules (5 mm in diameter) were used as charge containers. In order to examine the effects of the degree of supercooling and the cooling rate on chemical compositions of the crystals, two temperature programs were applied; after the charges were completely melted at temperatures  $30\text{--}40^\circ\text{C}$  above the liquidus temperatures for 3 hours, the charge was either (1) dropped rapidly (approximately  $2000^\circ\text{C/hr}$ ) to a desired isothermal crystallization temperature below the liquidus with the degree of supercooling,  $\Delta T$  of 10 to  $250^\circ\text{C}$  and then quenched into water after a desired duration (Table 1-A,C,D), or (2) cooled at a desired, constant cooling rate of 0.33 to  $530^\circ\text{C/hr}$  and then quenched into water at a desired temperature (Table 1-B,E). The former is called "isothermal crystallization experiment," and the latter "continuous cooling experiment." More detailed descriptions are given in the previous paper (Tsuchiyama, 1983). In order to compare with results of these crystallization experiments, heating experiments of annealed glasses of  $\text{Di}_{80}$ ,  $\text{Di}_{64}$ , and  $\text{Di}_{50}$  and of the  $\text{Di}_{80}$  glass were also conducted (Table 1-F).

Quantitative analyses of diopside, anorthite and glass were made with a JEOL-5 electron probe microanalyzer with a focused beam, 15 kv accelerating voltage and  $0.02\ \mu\text{A}$  sample current. The intensities of only Al, Mg and Ca were measured and the total weight percent was made 100% on the basis of the correction method of Nakamura and Kushiro (1970). The analysis, in which intensities of all the cations (Si, Al, Mg and Ca) were measured, was independently made in order to obtain errors due to the partial analyses. There was no difference in the  $\text{Al}_2\text{O}_3$ , MgO and CaO contents between the two analyses.

### Results

Porphyritic texture is developed in the isothermal crystallization experiments with  $\Delta T$  less than about  $100^\circ\text{C}$  and in the continuous cooling experiments with cooling rates less than about  $100^\circ\text{C/hr}$  (Tsuchiyama, 1983). Diopside nucleates first and grows to phenocryst size followed by simultaneous crystallization of anorthite and diopside as groundmass in the melts of  $\text{Di}_{80}$  and  $\text{Di}_{64}$  compositions, whereas anorthite nucleates first and grows to a phenocryst size followed by simultaneous crystallization of diopside and anorthite as groundmass in the melt of  $\text{Di}_{50}$  composition. The nucleation of diopside and anorthite is always delayed under supercooled conditions.

Run conditions and results are summarized in Table 1. Representative analyses of diopside and anorthite are given in Tables 2 and 3, respectively. Diopside contains 0.5–1.3

wt.%  $\text{Al}_2\text{O}_3$  mainly as  $\text{CaAl}_2\text{SiO}_6$  (CaTs) component. The number of Ca atoms (per O = 6) in the diopside phenocrysts is less than unity, indicating that the diopside contains  $\text{MgSiO}_3$  (En) as well as CaTs in the solid solution. With increasing CaTs component the En component decreases. Anorthite contains 0.3–1.2 wt.% MgO. With increasing Mg, Si increases whereas Al decreases. The sum of

Table 1. Conditions and results of experiments

(A) $\text{Di}_{80}$ (Isothermal crystallization experiments)										
Run#	$\Delta T$ [ $^\circ\text{C}$ ]	Dur. [min]	$\text{Al}_2\text{O}_3$ [mol%]			$K_I$	$K_{Rim}$	$X$ [ $\mu\text{m}$ ]	Products	
			Di-Max	Di-Min	Liq-Max					
T082*	12	240	0.76	0.64	5.4	0.16	0.12	110	di,gl	
T083*	12	480	0.84	0.48	5.7	0.18	0.084	110	di,gl	
T084*	12	720	0.84	0.40	6.25	0.18	0.064	140	di,gl	
T311	12	2880	0.76	0.36	n.d.	0.16	n.d.	410	di,gl	
T312	12	5760	0.60	0.46	n.d.	0.13	n.d.	n.d.	di,gl	
T201	22	973	0.96	0.56	5.85	0.21	0.096	160	di,gl	
T202	22	1093	0.96	0.50	6.35	0.21	0.079	100	di,gl	
T203	22	1230	0.98	0.52	6.1	0.21	0.085	160	di,gl	
T061*	32	60	1.28	1.02	7.1	0.28	0.14	37	di,gl	
T062*	32	120	1.40	0.80	7.85	0.30	0.10	44	di,gl	
T271	30	120	1.26	0.82	n.d.	0.27	n.d.	92	di,gl	
T063*	32	180	1.32	0.82	7.2	0.28	0.11	33	di,gl	
T064*	32	240	1.28	0.78	7.05	0.28	0.11	44	di,gl	
T273	30	360	1.26	0.66	6.55	0.27	0.10	57	di,gl	
T321	33	905	1.30	0.68	6.95	0.28	0.098	n.d.	di,gl	
T141	40	105	1.50	0.90	n.d.	0.32	n.d.	47	di,gl	
T143	40	150	1.46	0.94	n.d.	0.32	n.d.	n.d.	di,gl	
T022*	46	30	1.60	1.30	8.2	0.35	0.16	27	di,gl	
T023*	46	60	1.60	1.00	8.15	0.35	0.12	28	di,gl	
T024*	46	120	1.62	0.98	8.0	0.35	0.12	25	di,gl	
T134	49	150	1.78	1.08	n.d.	0.38	n.d.	44	di,gl	
T331	51	300	1.78	1.00	7.75	0.38	0.13	n.d.	di,gl	
T251	69	35	2.72	2.04	9.2	0.59	0.22	8.6	di,gl	
T253	69	70	2.78	2.14	8.9	0.60	0.24	12	di,gl	
T254	69	100	2.54	2.06	8.7	0.55	0.24	9.5	di,gl	
T071*	85	<1	3.06	2.60	8.45	0.66	0.31	6.7	di,gl	
T072*	85	20	2.96	1.98	8.9	0.64	0.22	7.2	di,gl	
T073*	85	40	3.06	1.58	9.55	0.66	0.17	6.2	di,gl	
T074*	85	60	2.98	1.56	9.35	0.64	0.17	7.0	di,gl	
T244	92	240	2.60	1.52	10.4	0.56	0.15	9.7	di,gl	
T391	90	964	2.84	1.28	9.95	0.61	0.13	n.d.	di,gl	
T282	109	40	3.14	2.01	n.d.	0.68	n.d.	6.0	di,gl	

(B) $\text{Di}_{80}$ (Continuous cooling experiments)											
Run#	dT/dt [ $^\circ\text{C/hr}$ ]	$T_0$ [ $^\circ\text{C}$ ]	$\text{Al}_2\text{O}_3$ [mol%]			$K_C$	$X$ [ $\mu\text{m}$ ]	$T_N(X)$ [ $^\circ\text{C}$ ]	$T_N(K)$ [ $^\circ\text{C}$ ]	Products	
			Di-Max	Di-Min	Liq-Max						
C033	0.33	1304	0.44	0.98	6.3	0.094	370	1316	1326	di,gl	
C013	1.3	1293	0.58	1.26	7.4	0.13	240	1313	1322	di,gl	
C014	1.3	1279	0.58	1.68	7.85	0.13	190	1311	1322	di,gl	
C061	1.3	1262	0.72	2.74	9.35	0.16	250	1313	1318	di,gl	
C062	1.3	1236	0.76	2.92	10.6	0.16	88	1302	1316	di,gl	
C063	1.3	1204	0.76	4.50	12.8	0.16	70	1299	1317	di,gl	
C131	1.3	1166	0.62	6.02	n.d.	0.13	n.d.			di,an,gl	
C052	8.0	1259	1.10	2.28	9.3	0.24	57	1296	1304	di,gl	
C072	8.2	1186	0.84	5.24	12.9	0.18	69	1299	1314	di,gl	
C073	8.2	1160	0.84	4.44	n.d.	0.18	60	1297	1314	di,an,gl	
C074	8.2	1160	0.98	4.78	n.d.	0.21	86	1302	1308	di,an,gl	
C103	8.9	1120	1.76	2.84	12.7	0.38	11	1256	1283	di,gl	
C022	20	1281	1.34	1.86	8.05	0.29	27	1282	1296	di,gl	
C023	20	1261	2.34	2.62	8.8	0.50	7.3	1242	1268	di,gl	
C081	31	1211	1.30	2.34	11.05	0.28	11	1257	1297	di,gl	
C082	31	1181	2.42	3.26	11.3	0.52	8.0	1246	1266	di,gl	
C083	31	1141	1.42	4.90	n.d.	0.31	12	1261	1294	di,an,gl	
C084	31	1098	2.62	3.22	n.d.	0.57	6.1	1235	1261	di,gl	
C042	120	1260	2.14	2.94	8.4	0.46	9.2	1251	1272	di,gl	
C092	120	1179	2.90	3.32	9.75	0.63	4.7	1222	1251	di,gl	
C094	120	1131	2.78	3.32	10.9	0.60	2.8	1192	1256	di,gl	

(C) $\text{Di}_{64}$ (Isothermal crystallization experiments)										
Run#	T [ $^\circ\text{C}$ ]	Dur. [min]	$\text{Al}_2\text{O}_3$ [mol%]			$K_I$	$K_{Rim}$	Products		
			Di-Max	Di-Min	Liq-Max					
T942	11	2880	2.78	1.34	9.9	0.31	0.14	di,gl		
T944	11	11520	2.52	1.14	9.6	0.28	0.12	di,an,gl		
T931	23	1442	3.50	2.38	10.65	0.39	0.22	di,an,gl		
T932	23	2880	3.54	2.22	10.05	0.40	0.22	di,an,gl		
T923	31	360	4.06	3.10	11.0	0.46	0.28	di,gl		
T961	51	45	5.88	4.97	12.1	0.66	0.41	di,gl		
T964	51	360	5.96	3.36	n.d.	0.67	n.d.	di,an,gl		
T993	80	10	6.92	5.98	12.45	0.78	0.48	di,gl		
T994	80	20	6.78	6.26	12.35	0.76	0.51	di,gl		
T1114	109	515	7.32	6.79	n.d.	0.82	n.d.	di,an,gl		

All the charges were melted at temperatures  $30\text{--}40^\circ\text{C}$  above the liquidus temperature (about  $1330$ ,  $1270$  and  $1360^\circ\text{C}$  for  $\text{Di}_{80}$ ,  $\text{Di}_{64}$  and  $\text{Di}_{50}$ , respectively) for 3 hours before isothermal crystallization or continuous cooling (A-E).

Table 1. (cont.)

(D) Di50 (Isothermal crystallization experiments)								
Run#	$\Delta T$ [°C]	Dur. [min]	MgO [mol%]			$K_I$	$K_{Rim}$	Products
			An-Max	An-Min	Liq-Max			
T671	37	11281	0.83	0.57	14.2	0.068	0.040	an,gl
T723	47	180	0.95	0.86	13.85	0.078	0.062	an,gl
T724	47	360	0.96	0.80	n.d.	0.079	n.d.	an,gl
T691	48	720	1.00	0.78	n.d.	0.082	n.d.	an,gl
T692	48	1440	0.93	0.74	13.95	0.076	0.053	an,gl
T693	48	2880	0.99	0.73	13.95	0.081	0.052	an,gl
T694	48	3720	1.02	0.67	14.5	0.084	0.046	an,gl
T681	49	11603	0.84	0.54	14.35	0.069	0.038	an,gl
T771	69	360	1.12	0.92	15.0	0.092	0.061	an,gl
T772	69	1440	1.10	0.82	15.25	0.090	0.054	an,gl
T773	69	2880	0.99	0.76	15.00	0.081	0.051	an,gl
T622	87	60	1.42	1.11	14.85	0.12	0.075	an,gl
T623	87	120	1.40	1.01	15.2	0.12	0.066	an,gl
T624	87	240	1.36	1.05	15.35	0.11	0.068	an,gl
T813	84	500	1.29	1.00	15.0	0.11	0.067	an,gl
T814	84	1230	1.23	0.95	15.5	0.10	0.061	an,gl
T741	85	2821	1.36	0.80	15.65	0.11	0.051	an,gl
T631	117	45	1.83	1.52	16.05	0.15	0.10	an,gl
T653	117	180	1.79	1.27	16.65	0.15	0.076	an,gl
T654	117	360	1.82	1.17	16.3	0.15	0.072	an,di,gl

(E) Di50 (Continuous cooling experiments)								
Run#	dT/dt [°C/hr]	$T_Q$ [°C]	MgO [mol%]			$K_C$	Products	
			Di-Max	Di-Min	Liq-Max			
C312	1.3	1315	0.66	0.78	12.9	0.054	an,gl	
C313	1.3	1284	1.00	1.10	14.35	0.082	an,gl	
C314	1.3	1254	0.66	1.06	15.85	0.054	an,gl	
C321	1.3	1215	0.64	0.98	n.d.	0.053	an,di,gl	
C322	1.3	1183	0.62	1.18	n.d.	0.051	an,di,gl	
C323	1.3	1152	0.70	1.18	n.d.	0.058	an,di,gl	
C324	1.3	1118	0.74	1.10	n.d.	0.061	an,di,gl	
C414	6.9	1253	1.12	1.26	15.95	0.092	an,gl	
C401	6.8	1216	1.00	1.64	17.4	0.082	an,gl	
C373	30	1285	1.10	1.34	13.8	0.090	an,gl	
C374	30	1254	1.02	1.58	15.25	0.084	an,gl	
C381	31	1214	1.18	1.70	16.9	0.097	an,gl	
C331	130	1229	1.64	2.24	16.4	0.14	an,gl	
C342	130	1204	1.88	2.72	17.05	0.15	an,gl	
C332	130	1184	2.32	2.76	18.05	0.19	an,gl	
C333	130	1143	2.14	2.60	n.d.	0.18	an,di,gl?	
C334	130	1143	1.38	2.08	n.d.	0.11	an,di,gl?	
C344	130	1116	1.84	2.16	n.d.	0.15	an,di,gl?	
C362	530	1042	1.84	2.82	n.d.	0.15	an,di,gl	
C364	530	978	2.60	3.62	n.d.	0.21	an,di,gl	

(F) Equilibrium experiments								
Run#	S.M.	Temp. [°C]	Dur. [min]	$\text{Al}_2\text{O}_3$ [mol%]			$K_{Rim}$	Products
				Di-Max	Di-Min	Liq-Max		
Q05	Di80(G)	1332	1560	0.61	0.26	4.8	0.054	di,gl
Q03	Di80(G)	1326	1420	0.54	0.30	5.05	0.059	di,gl
Q07	Di80(G)	1323	1560	0.61	0.28	5.2	0.054	di,gl
Q07	Di80(X)	1300	13020	0.64	0.56	6.4	0.088	di,gl
Q27	Di64(X)	1260	16170	1.60	0.82	9.1	0.090	di,an,gl

Run#	S.M.	Temp. [°C]	Dur. [min]	MgO [mol%]			$K_{Rim}$	Products
				Di-Max	Di-Min	Liq-Max		
Q63	Di50(G)	1357	5112	0.66	0.28	12.2	0.023	an,gl

$K_I$  : partition coefficient (crystal core)/(initial liquid)  
 $K_C$  : partition coefficient (crystal core)/(initial liquid)  
 $K_{Rim}$  : partition coefficient (crystal core)/(liquid near the interface)  
dT/dt : cooling rate  
 $T_Q$  : quench temperature  
X : average spacing between diopside crystals (dendrite arms)  
S.M. : starting materials G = glass  
X = annealed glass (crystalline)  
Products : di = diopside, an = anorthite, gl = glass  
\* : Pt-Au capsules were used.  
n.d. : not determined

If chemical compositions of diopside and melts are plotted in the ternary diagram  $\text{Al}_2\text{O}_3\text{-CaO-MgO}$ , they form an approximately straight line which is slightly different from the diopside-anorthite (or diopside-CaTs) join due to crystallization of the pyroxene containing the En component. We can thus regard the crystallization system in the experiments as a type of binary system, which mimics the diopside-anorthite join. For simplicity, only  $\text{Al}_2\text{O}_3$  contents in the diopside are used to represent the diopside compositions, and MgO contents are used to represent plagioclase compositions.

### Al contents of diopside

Diopside crystals are zoned. In the isothermal crystallization experiments, the Al content of diopside phenocrysts decreases from core to rim (Fig. 1a), whereas in the continuous cooling experiments the Al content increases from core to rim (Fig. 1b). Based on the phase diagram (Yoder, 1976, Fig. 5-2), Al content in diopside should increase as temperature falls, thus, the zoning obtained in isothermal crystallization is called "reverse zoning". Diopside in the groundmass is not homogeneous, but its zoning pattern does not appear to be systematic.

Table 2. Representative analyses of diopside phenocrysts

Di80												
$\Delta T$ (Temp.)	12(1318°C)		33(1297°C)		51(1279°C)		92(1238°C)					
Duration	2880 min		905 min		300 min		240 min					
	core	rim	core	rim	core	rim	core	rim				
$\text{SiO}_2$	55.15	55.28	54.64	54.87	53.87	54.69	53.02	53.50				
$\text{Al}_2\text{O}_3$	1.19	0.72	2.23	1.49	3.29	1.90	4.77	2.86				
MgO	19.12	18.94	18.41	18.44	17.89	18.07	17.48	17.80				
CaO	24.54	25.06	24.72	25.20	24.95	25.34	24.37	25.85				
Si	1.979	1.987	1.961	1.973	1.936	1.967	1.905	1.931				
Al	0.050	0.031	0.095	0.063	0.139	0.080	0.202	0.121				
Mg	1.023	1.015	0.985	0.989	0.959	0.969	0.936	0.957				
Ca	0.944	0.965	0.951	0.971	0.961	0.977	0.952	0.999				
Total	3.996	3.998	3.992	3.996	3.995	3.993	3.995	4.009				

Di80												
dT/dt	1.3°C/hr		1.3°C/hr		8.0°C/hr		120°C/hr					
Temp.	1262°C		1204°C		1259°C		1260°C					
	core	rim	core	rim	core	rim	core	rim				
$\text{SiO}_2$	54.53	52.51	54.67	51.24	54.42	53.53	53.31	52.76				
$\text{Al}_2\text{O}_3$	1.58	4.99	1.61	7.64	2.20	4.03	4.03	5.08				
MgO	18.68	16.18	19.11	15.79	18.28	17.22	17.73	16.94				
CaO	25.21	26.32	24.60	25.32	25.10	25.22	25.23	25.23				
Si	1.963	1.896	1.964	1.845	1.957	1.925	1.918	1.898				
Al	0.067	0.212	0.068	0.324	0.093	0.171	0.171	0.215				
Mg	1.002	0.871	1.024	0.848	0.980	0.923	0.935	0.909				
Ca	0.972	1.018	0.947	0.977	0.967	0.972	0.973	0.972				
Total	4.004	3.998	4.002	3.993	3.997	3.990	3.996	3.994				

Di64												
T (Temp.)	11(1259°C)		31(1239°C)		51(1219°C)		99(1171°C)					
Duration	2880 min		360 min		360 min		515 min					
	core	rim	core	rim	core	rim	core	rim				
$\text{SiO}_2$	52.48	53.33	51.44	52.63	49.12	52.16	48.08	48.47				
$\text{Al}_2\text{O}_3$	5.06	4.16	7.35	5.67	10.61	6.13	12.79	12.00				
MgO	17.48	17.41	16.45	17.14	15.36	16.23	14.08	14.49				
CaO	24.98	25.10	24.76	24.55	24.91	25.49	25.05	25.04				
Si	1.889	1.918	1.849	1.889	1.769	1.878	1.732	1.746				
Al	0.215	0.176	0.311	0.240	0.451	0.260	0.543	0.509				
Mg	0.938	0.933	0.882	0.917	0.825	0.871	0.756	0.778				
Ca	0.963	0.967	0.954	0.944	0.961	0.983	0.966	0.966				
Total	4.004	3.994	3.995	3.991	4.006	3.992	3.997	3.999				

0 = 6

the numbers of Si, Al and Mg atoms (per O = 8) is approximately three (T-atom in Table 3). These results can be explained by the substitution by  $\text{CaMgSi}_3\text{O}_8$  (Bruno and Facchinelli, 1975; Longhi et al., 1976; Beaty and Albee, 1980). The substitution by  $\text{CaSi}_4\text{O}_8$  (Beaty and Albee, 1980) might also take place because the number of Ca atoms is usually less than unity.

Table 3. Representative analyses of anorthite phenocrysts

Di50						
T(Temp.)	37(1323°C)		69(1291°C)		117(1243°C)	
Duration	1281 min		1440 min		180 min	
	core	rim	core	rim	core	rim
SiO <sub>2</sub>	44.44	44.27	44.51	44.31	45.31	45.00
Al <sub>2</sub> O <sub>3</sub>	35.13	35.52	34.78	35.02	33.65	34.14
MgO	0.45	0.35	0.59	0.54	1.08	0.76
CaO	19.98	19.86	20.12	20.13	19.96	20.10
Si	2.054	2.046	2.059	2.050	2.094	2.081
Al	1.914	1.934	1.896	1.910	1.833	1.861
Mg	0.031	0.024	0.041	0.038	0.075	0.053
Ca	0.990	0.984	0.997	0.998	0.988	0.996
Total	4.989	4.984	4.993	4.995	4.988	4.989
T-atom	3.999	4.004	3.996	3.997	4.001	3.994

Di50						
dT/dt	1.3°C/hr		6.8°C/hr		130°C/hr	
Temp.	1254°C		1216°C		1229°C	
	core	rim	core	rim	core	rim
SiO <sub>2</sub>	46.07	46.08	44.91	45.18	46.55	46.88
Al <sub>2</sub> O <sub>3</sub>	33.70	33.42	34.73	34.22	32.60	31.48
MgO	0.47	0.62	0.60	0.85	1.12	1.63
CaO	19.75	19.87	19.77	19.74	19.73	20.01
Si	2.123	2.215	2.073	2.086	2.146	2.165
Al	1.830	1.817	1.890	1.862	1.771	1.713
Mg	0.033	0.043	0.041	0.059	0.077	0.112
Ca	0.975	0.982	0.978	0.977	0.974	0.990
Total	4.962	4.966	4.982	4.983	4.969	4.979
T-atom	3.986	3.985	4.004	4.006	3.994	3.989

T-atom = Si+Al+Mg  
O = 8

The Al content of the crystal adjacent to the crystal-liquid interface is not constant even in a single crystal. The residual liquid adjacent to the interface is also not homogeneous and its composition depends on the composition of the adjacent diopside; the liquid with the lower Al content is in contact with diopside with higher Al content, and *vice versa* (Fig. 2). It cannot be verified by the electron probe micro-analyzer whether or not the crystal and the liquid just at the interface are homogeneous in composition. The isochemical lines of the liquid appear to intersect the corners of the crystal (Fig. 2) and can be interpreted as the Berg effect (Kern, 1953). Overlapping of diffusion fields in the melt of smaller crystals near the larger crystal complicates this interpretation, however, intersection of any isochemical line with the crystal indicates that the composition of the liquid would not be the same at the interface. Because of the compositional correlation between the crystal and the liquid near the interface, the composition of the crystal at the interface also seems likely to be varied. Although there is the heterogeneity of the crystal composition at the interface, clear sector zoning cannot be detected.

The ranges of Al content in diopside phenocrysts in a single charge of the isothermal crystallization experiments were obtained as a function of run duration (Fig. 3) and temperature (Fig. 4a). The most Al-rich and Al-poor compositions appear in the cores and rims of crystals, respectively (i.e., reverse zoning). For the charges of Di80 composition, the most Al-rich composition is approximately constant, whereas the most Al-poor composition decreases with increasing the run duration, and then becomes con-

stant (Fig. 3). Little systematic difference is detected between the runs using the Pt-wire loops and the Pt90Au10 capsules. It is seen from Figure 4a that the most Al-rich and Al-poor compositions increase with decreasing temperature, but the trend of the most Al-rich composition for Di80 is different from that for Di64.

Small crystals (20–80  $\mu\text{m}$  in diameter) formed in the heating experiments of the Di80 glass (1323–1332°C) are equant in shape and heterogeneous in composition. The Al contents of these crystals are slightly smaller than those formed in the isothermal crystallization experiments at 1320°C (Fig. 4a). In heating experiments of annealed Di80 glass, euhedral diopside crystals (the size increased from a few  $\mu\text{m}$  to about 10  $\mu\text{m}$  after heating) were observed, and indicate recrystallization during heating. Diopside crystals formed in this manner are too small to analyze and check for compositional heterogeneity. The Al contents of the crystals are similar to the most Al-poor composition of the crystals formed in the isothermal crystallization experiments at the same temperature, 1300°C (Fig. 4a).

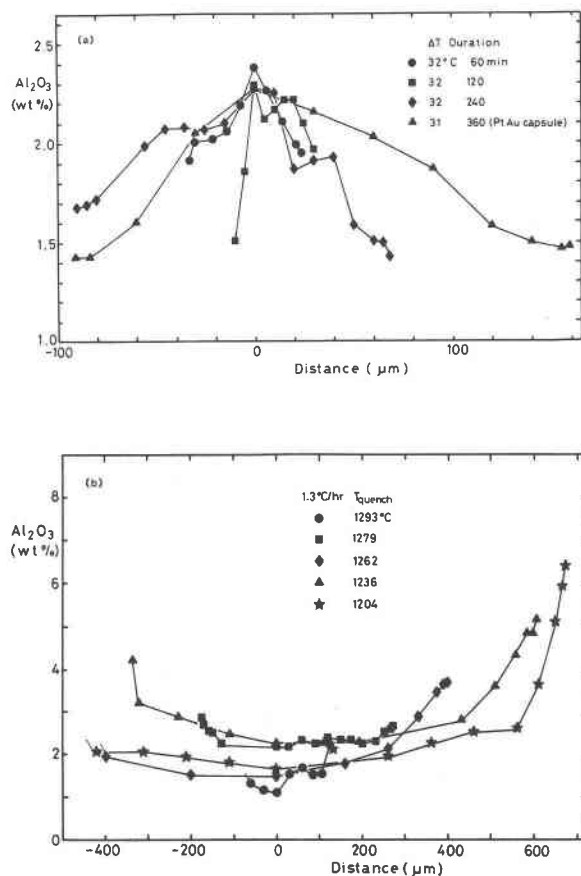


Fig. 1. Zoning profiles of Al<sub>2</sub>O<sub>3</sub> wt.% in diopside phenocrysts grown from the melt of Di80. (a) Isothermal crystallization experiments. (b) Continuous cooling experiments. Run conditions are given in each figure. Position with the maximum and minimum Al<sub>2</sub>O<sub>3</sub> contents are taken as the center of each crystal for (a) and (b), respectively.

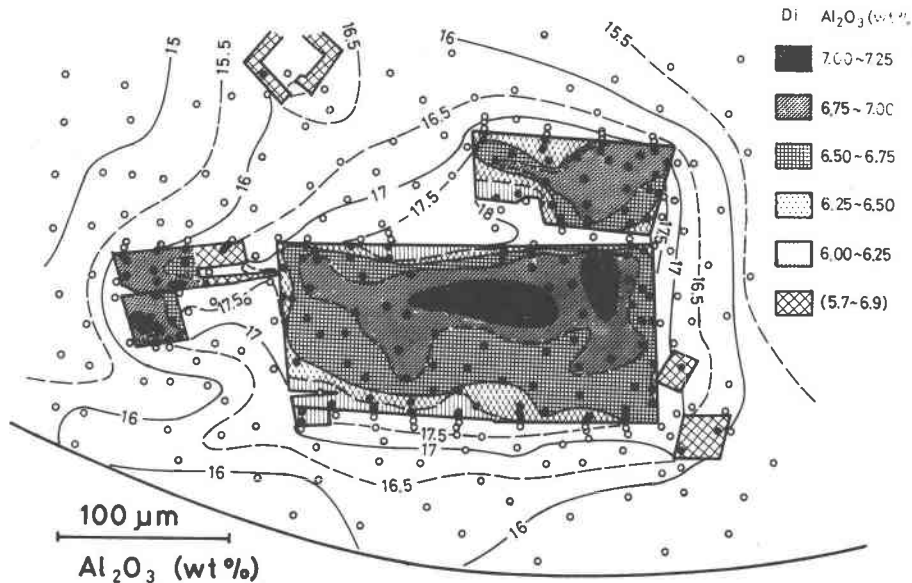


Fig. 2. Compositional map of  $\text{Al}_2\text{O}_3$  wt.% around diopside phenocrysts in the isothermal crystallization experiment using Di64 (Run # T923;  $\Delta T = 31^\circ\text{C}$ , run duration is 360 min).

In the continuous cooling experiments, the most Al-poor, al-rich compositions appear in the core and rim, respectively (i.e., normal zoning). They are given in the temperature- $\text{Al}_2\text{O}_3$  mole % diagram for the charges of Di80 composition (Fig. 4b). Although the Al content in the core for a given cooling rate is scattered, it increases with increasing cooling rate; it is about 0.4, 0.6–0.8, 0.8–1.1 and  $>1.1$   $\text{Al}_2\text{O}_3$  mole % for the cooling rates of 0.33, 1.3, 8.0–8.9, and 20–30 $^\circ\text{C/hr}$ , respectively. Except for some runs, especially those with rapid cooling rates, the Al con-

tent at the rim increases with decreasing temperature; for example, it increases from 1.2 to 6 mole % at 1.3 $^\circ\text{C/hr}$  with decreasing the quench temperature from 1279 to 1166 $^\circ\text{C}$  (Fig. 4b). The exceptions are probably due to the difficulties of the complete determination of the rim compositions in very fine crystals of diopside.

Several compositions of diopside in the groundmass were also obtained in the isothermal cooling experiments for Di80. Their ranges are about 1.4–3.6 and 1.7–3.0  $\text{Al}_2\text{O}_3$  mole % for the charges cooled at 1.3 $^\circ\text{C/hr}$  quenched at 1166 $^\circ\text{C}$  and cooled at 20 $^\circ\text{C/hr}$  quenched at 1160 $^\circ\text{C}$ , respectively (Fig. 4b). The Al contents in the groundmass diopside are less than those at the rim of the phenocrysts.

### Mg contents in anorthite

The zoning patterns of Mg content in anorthite phenocrysts are not as evident as the Al content in diopside phenocrysts. Many crystals are zoned with Mg content decreasing from core to rim during isothermal crystallization, and increasing from core to rim during continuous cooling.

In the isothermal crystallization experiments for Di50, the most Mg-rich composition, which appears in the core, is constant in a single charge at a given temperature, and increases with decreasing temperature (Table 1). The most Mg-poor composition at the rim decreases with increasing run duration and does not become constant. In the continuous cooling experiments, the Mg content in the core increases as cooling rate is increased (Table 1).

### Theory

The partitioning of elements between crystal and liquid during crystal growth is controlled mainly by crystal-liquid interface attachment kinetics and/or diffusion of components in the liquid (Burton et al., 1953; Tsuchiyama et al.,

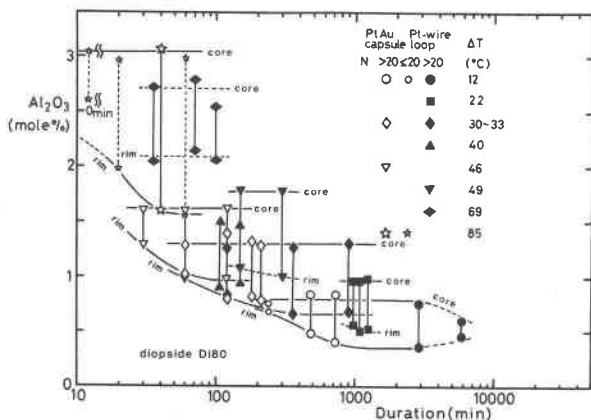


Fig. 3. Variation of the  $\text{Al}_2\text{O}_3$  content (mole%) of diopside phenocrysts with run duration in the isothermal crystallization experiments using Di80. The maximum and minimum values are given. Because of the reverse zoning, the maximum and minimum values correspond to the core and rim compositions, respectively. Experimental conditions are given in the figure. Smaller symbols show that number of data  $N$  is less than or equal 20.

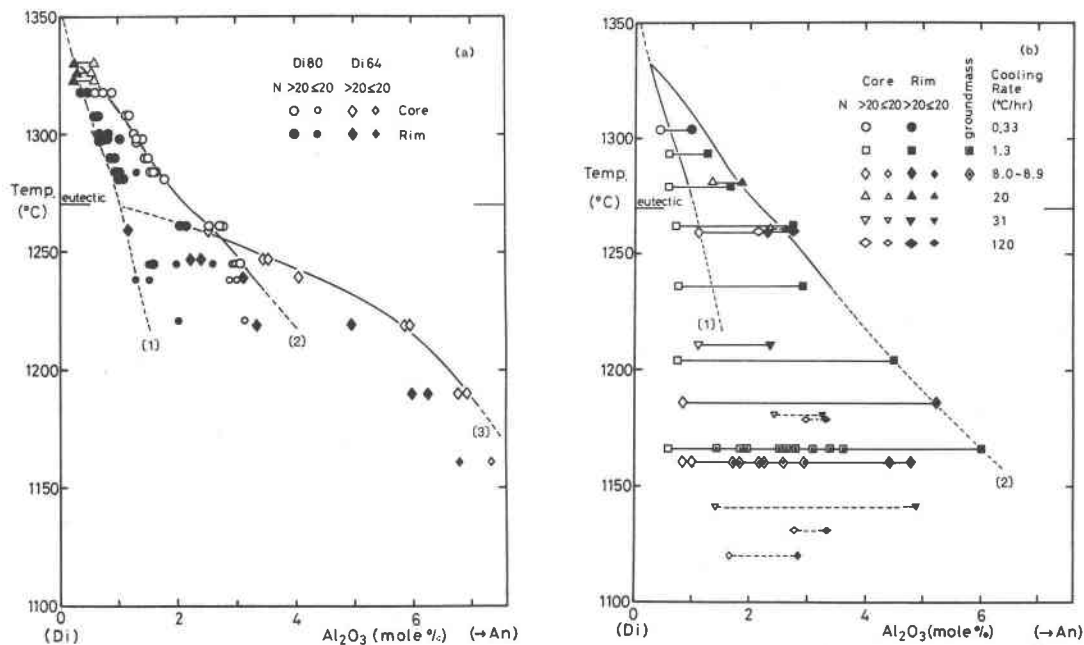


Fig. 4. The core (open symbols) and rim (solid symbols) compositions of diopside phenocrysts plotted on the crystallization temperature— $\text{Al}_2\text{O}_3$  mole% diagram. Curves (1) and (2) show equilibrium composition and initial composition, respectively, in the isothermal crystallization experiments using Di80. Initial composition for Di64 is also given as curve (3). Smaller symbols show that number of data  $N$  is less than or equal 20. (a) Isothermal crystallization experiments using Di80 (circles) and Di64 (diamonds). Results of the heating experiments of the annealed Di80 glass at  $1300^\circ\text{C}$  (an upward triangle) and the Di80 glass (downward triangles) are also shown. (b) Continuous cooling experiments using Di80. Cooling rates are given in the figure. Compositions of groundmass diopside are also given.

1981) as well as by crystal growth processes (e.g., Kirkpatrick, 1981). The interaction of interface kinetics and diffusion process is modeled by theory in which the liquid of the composition,  $X_L$ , is rapidly supercooled to the temperature,  $T_C$ , with the initial supercooling,  $\Delta T$ , and crystallization takes place at the constant temperature in a binary system (Fig. 5a). Profiles of temperature and composition near the interface during the growth (Fig. 5b,c) are constructed, on the basis of the previous theory for solidification of metals (e.g., Tarshis and Tiller, 1967). In the present model, temperature is assumed to be uniform through the charge, and in general, local equilibrium at the interface is not maintained. The actual composition of the liquid,  $X_L^i$ , at the interface is different from the composition of the liquidus,  $X_L^e$ , and the actual temperature,  $T_C$ , is different from the liquidus temperature,  $T_L^i$ . The difference of composition or temperature,  $\Delta X_1 = X_L^e - X_L^i$  (Fig. 5b) or  $\Delta T_1 = T_L^i - T_C$  (Fig. 5c), can be regarded as the driving force for crystal growth at the interface. The difference,  $\Delta X_M = X_L^i - X_L$  or  $\Delta T_M = T_L - T_L^i$ , is the driving force for growth by diffusion in the liquid. The composition of the crystal at the interface,  $X_S^i$ , is determined by the interface kinetics using the interface partition coefficient,  $K_1$  ( $K_1 = X_S^i/X_L^i$ ) which is a function of  $\Delta X_1$  or  $\Delta T_1$  (Baker and Cahn, 1971).

If diffusion in the liquid is much slower than the inter-

face kinetics then growth is controlled solely by diffusion, that is, interface equilibrium is maintained. In this case, the compositions of the crystal and the liquid at the interface,  $X_S^i$  and  $X_L^i$ , must be constant and equal to the solidus and liquidus compositions,  $X_S^e$  and  $X_L^e$ , respectively during growth. Accordingly, the crystal is not expected to be zoned, having instead a uniform composition of the solidus,  $X_S^e$ . The equilibrium partition coefficient,  $K_0$ , is determined by  $X_S^e$  and  $X_L^e$  ( $X_S^e = K_0 X_L^e$ ).

Baker and Cahn (1971) discussed the possible range of solid composition (from  $X_1$  to  $X_4$  in Fig. 6) by interface kinetics in a binary system on the basis of thermodynamic theory. They divided this range into three regions in terms of chemical potential change by crystallization. In Region I the chemical potentials of both solute and solvent decrease (the crystal composition,  $X_S$ , is between  $X_2$  and  $X_3$  at the temperature,  $T_C$  in Fig. 6), in Region II the chemical potential of the solute increases (solute trapping;  $X_S = X_3 \sim X_4$ ), and in Region III the chemical potential of the solvent increases (solvent trapping;  $X_S = X_1 \sim X_2$ ). Hopper and Uhlmann (1974) pointed out two particular solid compositions with "maximum change in free energy" ( $X_M$  in Fig. 6; a slope of the tangent to  $G_S(X)$  at this point is equal to that to  $G_L(X)$  at  $X_L^i$ ) and "partial equilibrium at the interface" ( $X_E$  in Fig. 6; at this point, the line from  $X_L^i$  is tangent to  $G_S(X)$ ).

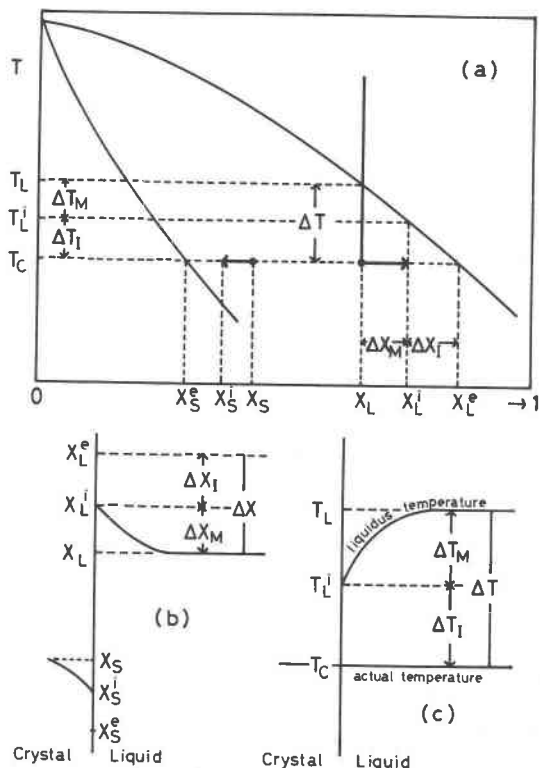


Fig. 5. (a) Schematic illustration of temperature and compositions of the crystal and the liquid when the liquid of the composition  $X_L$  is rapidly supercooled with  $\Delta T$  and crystal growth takes place at the constant temperature  $T_C$  in a binary system. (b) Compositional profile near the crystal-liquid interface. (c) Temperature profile near the crystal-liquid interface.

## Discussion

### Development of reverse zoning and significance of interface kinetics

Discussion of the development of reverse zoning in the isothermal crystallization experiments is based upon three assumptions. First, growth of diopside and anorthite phenocrysts occurs in a binary system. As previously discussed, this assumption appears to be valid for the growth of diopside because the compositions of the diopside phenocrysts and the residual liquid make an approximately linear trend slightly different from the diopside-anorthite join. Second, temperature is uniform throughout the charge. Because the thermal diffusivities are larger than the diffusion coefficients, removal of the latent heat of crystallization generated at the interface is probably of little significance (Kirkpatrick, 1981). In fact, actual measurements of temperature at the growing interface (Klein and Uhlmann, 1974) and computer simulations of plagioclase growth (Loomis, 1981; 1982) show that the temperature rise due to the latent heat is very small. Third, the diffusion of components in the crystal is so slow that compositions of the crystals are frozen once the crystal near the interface

is incorporated into the crystal interior. The diffusion coefficients for Al, Mg and Ca in diopside are approximately  $10^{-14} - 10^{-15} \text{cm}^2/\text{sec}$  at the temperature range in the present experiments (Freer et al., 1982). These values indicate that the detectable diffusion distance is less than  $1 \mu\text{m}$  even for the longest run (10 days).

If the growth of the crystal is controlled only by diffusion in liquid and interface equilibrium is attained, an unzoned crystal is expected to be formed as previously discussed. Although the compositional gradients in the liquid (Fig. 2) indicate that diffusion in the liquid is significant, the interface kinetics also play an important role because diopside and anorthite phenocrysts are reversely zoned in the isothermal crystallization experiments (Fig. 1a). Interface equilibrium also does not explain the compositional vari-

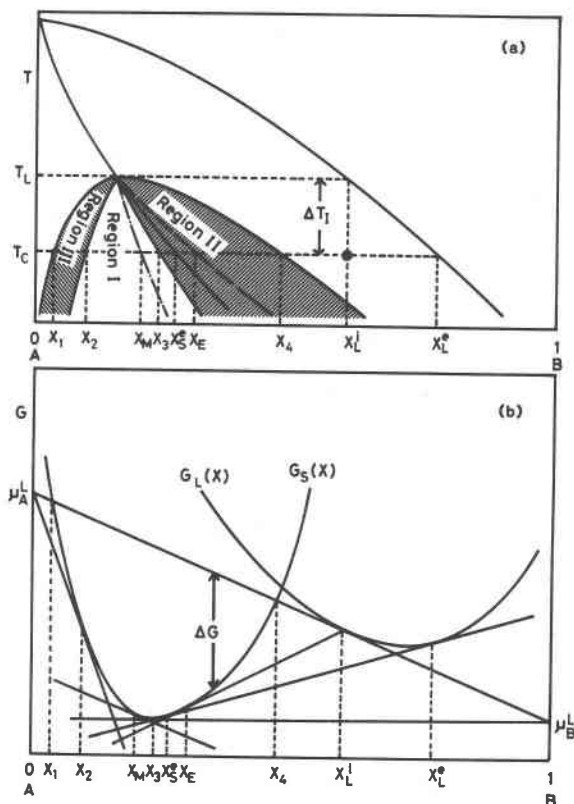


Fig. 6. Schematic phase diagram of a binary system A-B. When the liquid at the crystal-liquid interface  $X_L^i$  is supercooled with  $\Delta T_i$  at the temperature  $T_C$ , possible compositional range of the crystal grown in the liquid (from  $X_1$  to  $X_4$ ) is divided into three regions (Regions I, II and III) based on the thermodynamic considerations by Baker and Cahn (1971). Regions II and III are called "solute trapping" and "solvent trapping". (b) Free energy-composition curves for the crystal  $G_S(X)$  and for the liquid  $G_L(X)$  at the temperature  $T_C$ .  $\Delta G$  is the free energy change due to growth of infinitesimally small amounts of the crystal in the liquid with the composition  $X_L^i$ . The compositions of the crystal,  $X_M$  and  $X_E$ , are produced by the maximum change in  $\Delta G$  and by the partial equilibrium, respectively (Hopper and Uhlmann, 1974). See text for more detail.

ations of diopside and liquid near the interface (i.e., the liquid with the lower Al content is in contact with diopside with higher Al content at the interface, and *vice versa*) (Fig. 2). The composition of the liquid at the interface,  $X_L^i$ , is different from the liquidus composition,  $X_L^e$ , that is,  $\Delta X_L > 0$ .

Reverse zoning is produced in crystals in the following manner. A crystal nucleates from a supercooled melt (Fig. 5a) and starts to grow at a rate dependent on  $\Delta T$ . As crystallization proceeds, the melt will approach the equilibrium melt composition,  $X_L^e$ , causing the rate of growth to slow and finally cease. If the growing crystal incorporates excess amounts of the melt component, such as the composition of the crystal,  $X_S$ , than the equilibrium composition,  $X_S^e$  ( $X_S$  from  $X_L^i$  at the beginning of the growth,  $X_S^i$  from  $X_L^i$ , and finally  $X_S^e$  from  $X_L^e$ ), then reverse zoning is produced. This model is essentially the same model as proposed by Lofgren (1974) and Smith and Lofgren (1983) for major element reverse zoning in plagioclase and is verified by the results on the chemical compositions of the crystal and melt. These results stress the significance of interface kinetics on zoning.

The composition at the rim of the diopside crystals is Al-poor which decreases and then becomes constant as run duration increases for a given crystallization temperature for Di80 (Fig. 3). This final constant rim composition is similar to the composition of crystals produced in a reverse experiment where annealed Di80 glass is heated at 1300°C (downward triangle of Fig. 4a). This composition is considered to be the equilibrium composition at a given temperature (a kind of solidus in the relevant system) which in the final stages of crystallization signifies that equilibrium is maintained at the diopside-melt interface. The solidus for Di80 is shown in the temperature- $\text{Al}_2\text{O}_3$  mole % diagram (curve (1) of Fig. 4a). Although the composition of the liquid at the interface cannot be determined exactly, this composition appears to change from  $X_L$  to the equilibrium value,  $X_L^e$  (Tsuchiyama, in prep.).

The most Al-rich composition in the core of diopside can be assumed to be the composition of the initial crystal which starts to grow in the liquid of the starting material ( $X_S$  in Fig. 5a). These compositions are plotted in Figure 4a. Although it is difficult to directly measure precise values of the interface partition coefficient,  $K_I$ ,  $K_I$  can be estimated as a function of  $\Delta T_I$  by using the assumption of the initial composition (Fig. 7;  $\Delta T_I$  is equal to the initial super cooling,  $\Delta T$ ).  $K_I$  and deviation of  $K_I$  from  $K_0$  increase with increasing  $\Delta T$  (Fig. 7) and thus with  $\Delta T_I$ . The  $K_I$ - $\Delta T_I$  relation for diopside is affected by the liquid composition;  $K_I$  for Di80 is smaller than  $K_I$  for Di64 at the same  $\Delta T$ .

During the change in liquid composition (from  $X_L$  to  $X_L^e$ ) (Fig. 5a), the degree of supercooling at the interface,  $\Delta T_i$ , decreases from the initial value,  $\Delta T$ , to zero, and thus  $K_I$  decreases from the initial value,  $K_I(\Delta T)$  to the equilibrium value,  $K_0$ . The composition of the crystal successively grown is expected to change from the initial value,  $X_S =$

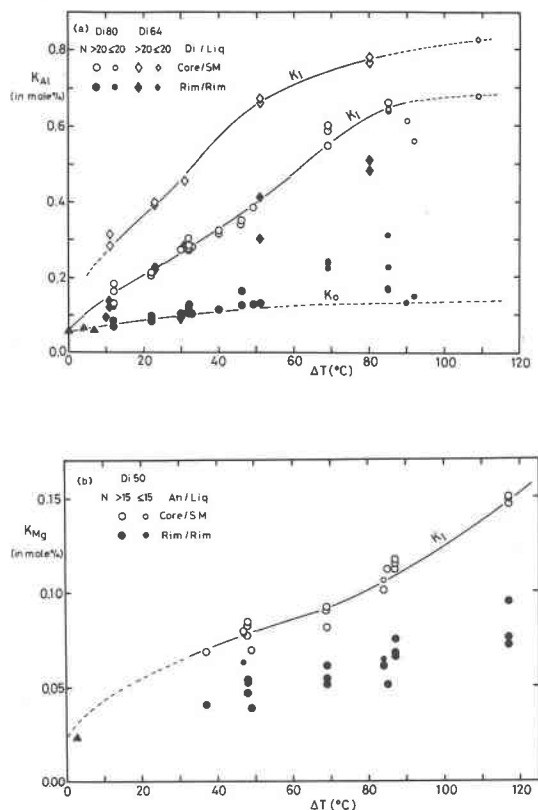


Fig. 7. Partition coefficients of elements between the core composition of crystal and liquid of the starting material (open symbols) plotted against  $\Delta T$  in the isothermal crystallization experiments. (a) Al partitioning between diopside phenocrysts and the melts of Di80 (circles) and Di64 (diamonds). The partition coefficients between the rim composition and the most Al-poor composition of the residual liquid are also plotted (solid symbols). Values obtained from the heating experiments of the annealed Di80 glass (an upward triangle) and the Di80 glass (downward triangle) are also given. (b) Mg partitioning between anorthite phenocrysts and melt of Di50. Smaller symbols show that number of data for diopside or liquid N is less than or equal to 20 for (a) and 15 for (b), respectively.

$X_L/K_I(\Delta T)$  to the solidus composition,  $X_S^e = X_L^e/K_0$ , and reverse zoning is formed at constant temperature. Diopside phenocrysts with the larger Al contents (larger  $X_S^i$ ) are in contact with the liquids with the smaller Al contents (smaller  $X_L^i$ , and thus larger  $\Delta T$ ) at the interface, and vice versa (Fig. 2). These results are also consistent with the above discussion on the development of the reverse zoning.

Formation of the reverse zoning and the incorporation of excess amounts of solute into the crystals (Al in diopside and Mg in anorthite) indicate that solute trapping (region II of Fig. 6) of Baker and Cahn (1971) takes place during the growth of crystals in these experiments. Regions I and III are eliminated because these regions are located below the equilibrium value,  $X_S^e$  (Fig. 6). For the same reason, the composition with "the partial equilibrium"  $X_E$  is possible,

but that with "the maximum change in free energy"  $X_M$  is not.

### Normal zoning in continuous cooling runs

Normal zoning is usually explained by assuming interface equilibrium. In the present experiments, normal zoning is also formed by interface kinetics. In fact, the Al contents in the core are sometimes greater than Al values predicted by equilibrium conditions (Fig. 4b).

Assuming that the partition coefficient  $K_C$  can be obtained at the beginning of the growth from the most Al-poor or Mg-poor composition in the core and the liquid of the starting material, it has a tendency to increase with increasing the cooling rate (Fig. 8). Nucleation of diopside and anorthite is delayed at the temperature  $T_N$  with the degree of supercooling  $\Delta T_N$  as depicted in Figure 9 (Tsuchiyama, 1983). If the initial composition of the crystal is assumed to be determined by the  $K_T\text{-}\Delta T_1$  relation, that is, by the initial composition line obtained in the isothermal crystallization experiments ( $X_S$  in Fig. 9), then with increasing cooling rate,  $\Delta T_N$  increases and  $K_C = K_T(\Delta T_N)$  increases.

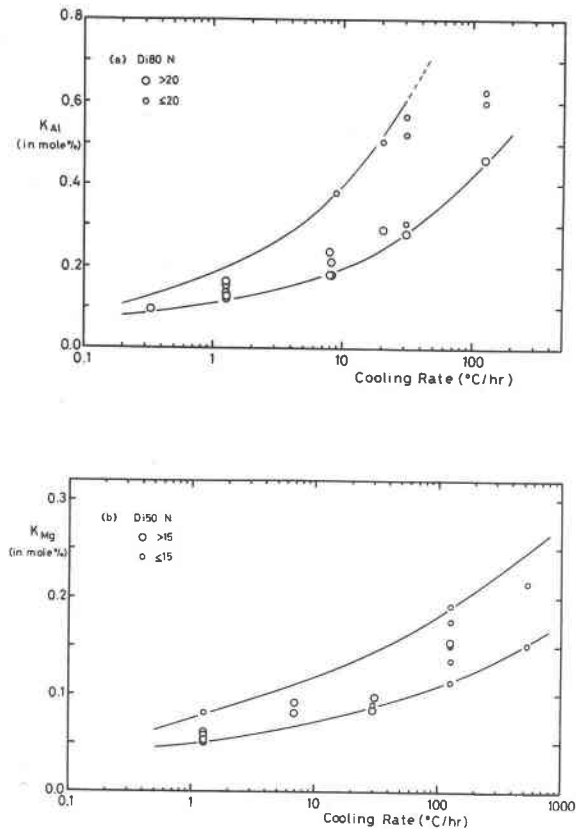


Fig. 8. Partition coefficient of elements between core composition of crystal and liquid of the starting material plotted against the cooling rate in the continuous cooling experiments. (a) Al partitioning between diopside phenocrysts and melt of Di80. (b) Mg partitioning between anorthite phenocrysts and melt of Di50. Smaller symbols show that number of data for diopside N is less than or equal 20 for (a) and 15 for (b), respectively.

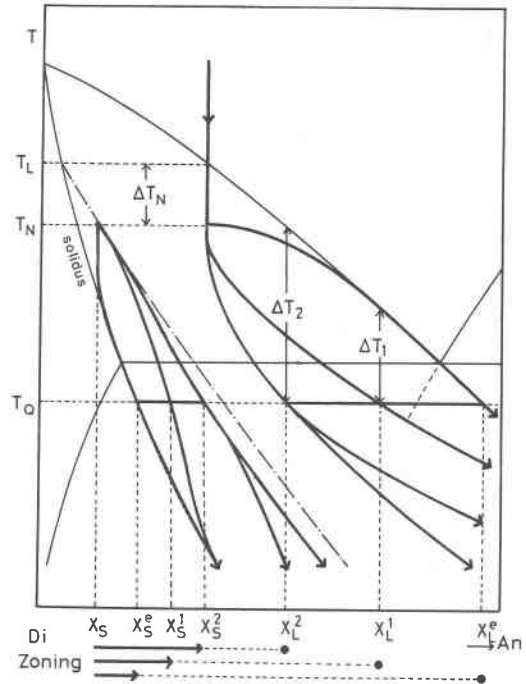


Fig. 9. Schematic illustration of the development of normal zoning in diopside phenocrysts produced by the continuous cooling experiments. The liquid is supercooled by  $\Delta T_N$  before nucleation of diopside. The composition of the crystal at the beginning of growth  $X_S$  is determined by the initial composition line obtained by the isothermal crystallization experiments (dotted curve). Curves show compositional trends of the crystal and liquid at several crystal-liquid interfaces. At temperature  $T_Q$  several ranges of the normal zoning, from  $X_S$  to  $X_S^e$ ,  $X_S^1$  and to  $X_S^2$ , are produced according to liquid compositions at the interface  $X_L^e$ ,  $X_L^1$  and  $X_L^2$ .

Because the values of  $\Delta T_N$  are scattered at the same cooling rate (Tsuchiyama, 1983),  $K_C$  is also variable.

With decreasing temperature, the crystal grows and the residual liquid develops compositional gradients around single crystals. Trends of the liquid compositions at the several interfaces are shown in Figure 9 (e.g.,  $X_L^e$ ,  $X_L^1$  and  $X_L^2$  at  $T_Q$ ). At the interface with the liquid composition,  $X_L^1$  (and thus  $\Delta T_1 = \Delta T_1$ , Fig. 9), the crystal grows with a composition of  $X_S^1 = X_L^1/K_T(\Delta T_1)$  (strictly speaking, the  $K_T\text{-}\Delta T_1$  relation in this case is somewhat different from that of Figure 7 because the liquid composition is different from that of the starting material). If  $X_S^1$  is greater than  $X_S$  as shown in Figure 9, the normal zoning (from  $X_S$  to  $X_S^1$ ) is formed at the temperature  $T_Q$ . Heterogeneity of the liquid composition at the interface produces various ranges of normal zoning (from  $X_S$  to  $X_S^e$ ,  $X_S^1$  and to  $X_S^2$  in Fig. 9) in a single crystal.

### Application

#### Evaluation of significance of interface kinetics.

The significance of interface kinetics in the experimental data on natural systems is obscure, primarily due to the

presence of additional components. The crystal-liquid equilibrium is complicated by an additional degree of freedom. Interface equilibrium is probably maintained for Fe/Mg partitioning between olivine and liquid produced in the isothermal crystallization experiments because the olivines are homogeneous (Donaldson et al., 1975) or the partition coefficients near the rim of olivine have equilibrium values (Walker et al., 1976). Minor element partitioning is more complex as excess amounts of minor elements should be incorporated into olivine by solute trapping. This is supported by the compositions of liquids near the interface, larger Ca/Mg partition coefficients than equilibrium values (Kirkpatrick et al., 1981) and a dependence of Ni/Mg partition coefficients on the growth rate of olivine (Kouchi et al., 1983b). Partitioning of Mg, Fe and Ca between pyroxene and liquid in some experiments indicates that interface equilibrium is maintained (Grove and Bence, 1977; Gamble and Taylor, 1980) but not in others done at rapid cooling rates (Grove and Bence, 1979). In a similar manner to olivine, solute trapping is important in the partitioning of minor elements (Al, Ti) (Grove and Raudsepp, 1978; Grove and Bence, 1977). Kouchi et al. (1983a) produced sector zoned clinopyroxene in isothermal crystallization, with Al and Ti reverse zoning in each sector. Reverse zoning was also produced in plagioclase in isothermal crystallization experiments in the system plagioclase- $\text{H}_2\text{O}$  (Lofgren, 1974). Solute trapping appears to be significant to the CaAl/NaSi partitioning, however, the effect of the third component,  $\text{H}_2\text{O}$ , on zoning (Loomis, 1981; 1982) needs further examination. Trace element partitioning for forsterite, diopside and anorthite grown from melts doped with REE exhibits kinetic effects and is probably caused by solute trapping (Lindstrom, 1983). In summary, interface equilibrium is maintained for major element partitioning in olivine and some pyroxenes, whereas the interface kinetics of solute trapping plays a significant role in the major element partitioning for other pyroxenes and plagioclase and in the minor element partitioning for olivine, pyroxene and plagioclase.

#### *Attainment of equilibrium in "equilibrium experiments"*

Many melting and/or crystallization experiments have been carried out to determine phase diagrams and partition coefficients of element between crystal and melt by measuring chemical compositions of product phases. In these "equilibrium" experiments it is important to evaluate attainment of equilibrium.

In a crystallization experiment, in which mineral(s) crystallizes from a melt (or heated glass) at a given constant temperature, interface kinetics will affect the compositions of crystals produced and the partition coefficients if the melt is strongly undercooled. In the present experiments, compositional zoning still remains in diopside and anorthite even if compositions of residual melts become homogeneous. Partition coefficients of rim-rim pairs may give erroneous results unless detailed zoning patterns, such as that shown in Figure 2, are determined.

Powders of minerals (or devitrified glass) are usually partially melted at a constant temperature during an "equilibrium" experiment. A melt with equilibrium composition is produced instantaneously and the residual crystal changes its composition by diffusion of elements through the crystal (Tsuchiyama and Takahashi, 1983). If a melt with equilibrium composition is produced instantaneously and recrystallization occurs from the melt, then the composition of that crystal is very close to an equilibrium composition.

It is easy to attain equilibrium if diffusion is fast or the effect of interface kinetics is very small. In cases where they are not (i.e., trace element partitioning between pyroxene and melt), melting experiments with recrystallization produces the best result as long as an equilibrium melt is produced instantaneously. Huebner and Turnock (1980) conducted experiments in which pyroxene crystals were partially melted and recrystallized, and compared the partition coefficients of trace elements between pyroxene and melt with those obtained from different experiments using different starting materials. The partition coefficients of Al and Ti from their experiments are similar to or smaller than the other experimental determinations (Table 4 in Huebner and Turnock, 1980). The larger partition coefficients reflect interface kinetic effects because excess amounts of Al and Ti are incorporated into pyroxene crystals.

Several criteria are used to confirm attainment of equilibrium: (1) Product phases are chemically homogeneous. (2) The experimental result is independent of starting material used and duration of the experiments. (3) The experimental charges approach a textural equilibrium with euhedral crystals in a melt. (4) The results are reproducible (e.g., Huebner and Turnock, 1980). All of these criteria are reasonable except for the third one. This criterion is only available if recrystallization takes place from melt with equilibrium composition, because euhedral crystals suggest nothing more than that they are products of crystallization from melt that is not greatly undercooled.

#### *Estimation of cooling rates from morphology and chemical composition of minerals*

There have been many experimental studies to estimate cooling rates of magmas from the morphology (e.g., shape, density and size of minerals) or chemical composition of minerals (e.g., Donaldson et al., 1975; Grove and Bence, 1977; Grove and Walker, 1977; Walker et al., 1978; Tsuchiyama et al., 1980).

Random nucleation apparently influences initial composition of crystals and the partition coefficient,  $K_C$ , as evidenced by the variable core compositions produced in the continuous cooling experiments (Fig. 8). It also probably affects the morphology of phenocrysts. The present experiments enable us to discuss this effect qualitatively by measuring the spacing between crystals or dendrite arms of diopside phenocrysts for Di80 (average spacing of ten different positions in a single charge were measured). In the isothermal crystallization experiments, the correlation of

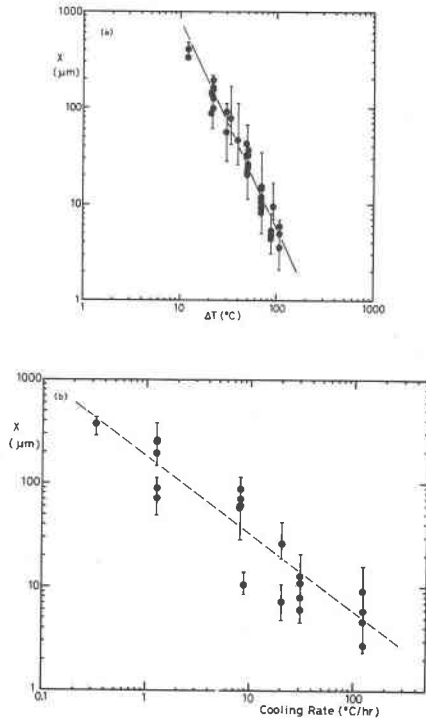


Fig. 10. The average spacing between crystals or dendrite arms of diopside phenocrysts  $X$ . (a)  $X$ - $\Delta T$  in the isothermal crystallization experiments for Di80. (b)  $X$ -cooling rate in the continuous cooling experiments for Di80. Bars indicate the maximum and minimum spacings.

the average spacing  $X$  and  $\Delta T$  appears to be good (Fig. 10a, the correlation coefficient,  $r = -0.959$  and  $X = 1.2 \times 10^5 \Delta T^{-2.2}$  in  $\mu\text{m}$ ), whereas the correlation between  $X$  and the cooling rate,  $dT/dt$ , is poor (Fig. 10b,  $r = -0.896$  and  $X = 180 dT/dt^{-0.76}$  in  $\mu\text{m}$ ) in the continuous cooling experiments. These results indicate that the average spacing is determined by  $\Delta T$ , and not by the cooling rate.

If  $K_C$  and  $X$  are determined by the degree of supercooling  $\Delta T_N$ , then at the time of the nucleation,  $\Delta T_N$  can be estimated independently from  $K_C$  (Fig. 8a) based on the  $K_C$ - $\Delta T_N$  relation (Fig. 7a) and from  $X$  (Fig. 10b) based on the  $X$ - $\Delta T$  relation (Fig. 10a) for each charge of Di80 composition (Fig. 11). Correlation of these values is good, but each point shifts slightly from the slope of unity and the  $\Delta T_N$  value estimated from  $X$  is greater than that from  $K_C$ . This correlation indicates that the core composition and the average spacing are approximately determined by the degree of supercooling  $\Delta T_N$  at the time of the nucleation. The deviation of the slope from unity is probably due to a higher value than the actual  $\Delta T_N$  estimated from the average spacing as some nucleation would take place at larger degrees of supercooling than  $\Delta T_N$ .

### Conclusion

1. Reverse zoning is produced during isothermal crystallization following instantaneous cooling due to the effect

of the interface kinetics in which excess amounts of elements are incorporated into crystals (Al in diopside phenocrysts and Mg in anorthite), whereas normal zoning is produced by continuous cooling even if the interface kinetics are significant.

2. Chemical compositions of the phenocrysts and residual liquid near the crystal-liquid interface are inhomogeneous, so that various compositional ranges of zoning are produced within a single crystal.

3. The partition coefficients of Al or Mg between core of the crystal and the initial liquid increase with increasing the degree of supercooling in the isothermal crystallization experiments. In the continuous cooling experiments the coefficients are more variable at the same cooling rate and tends to increase with increasing cooling rate.

4. Based on the results of previous experiments, kinetic effects on major element partitioning for olivine and some pyroxenes are insignificant, while the interface kinetics of "solute trapping" are important in major element partitioning for plagioclase and pyroxenes and in minor element partitioning for olivine, pyroxene and plagioclase.

5. Values of partition coefficients between crystal and melt which are determined by partial melting experiments, in which recrystallization takes place in an infinitesimally undercooled melt, are close to equilibrium values.

6. The core/initial liquid partition coefficient has a correlation with the morphology of phenocrysts in the continuous cooling experiments. The degree of supercooling at the time of nucleation but not the cooling rate can be estimated directly from the composition of the core or the morphology of the crystal.

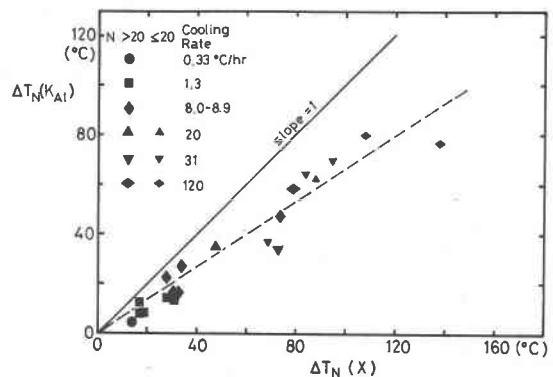


Fig. 11. The degree of supercooling at the time of nucleation of diopside phenocrysts estimated from the core composition  $\Delta T_N(K_{Al})$  plotted against that from the average spacing  $\Delta T_N(X)$  for each charge in the continuous cooling experiments for Di80. Smaller symbols show that number of data on the composition  $N$  is less than or equal 20.

### Acknowledgments

The author is grateful to Profs. I. Kushiro and Y. Nakamura of the University of Tokyo, Dr. G. Lofgren of NASA, Johnson Space Center, Dr. T. Grove of MIT, Dr. D. Gust of L.P.I. and Dr. M. Kitamura of Kyoto University for discussions and critical reading of the manuscript.

## References

- Albarede, F. and Bottinga, Y. (1972) Kinetic disequilibrium in trace-element partition between phenocrysts and host lava. *Geochimica et Cosmochimica Acta*, 36, 141–156.
- Baker, J. C. and Cahn, J. W. (1971) Thermodynamics of solidification. In *Solidification*, American Society for Metals, Metals Park, Ohio.
- Beatty, D. W. and Albee, A. L. (1980) Silica solid solution and zoning in natural plagioclase. *American Mineralogist*, 65, 63–74.
- Bianco, A. S. and Taylor, L. A. (1977) Application of dynamic crystallization studies: Lunar olivine normative basalts. *Proceedings of the Lunar Science Conference 8th*, 1593–1610.
- Brice, J. C. (1973) *The Growth of Crystals from Liquids*, p. 379. North-Holland Publishing Company, Amsterdam.
- Bruno, E. and Fachinelli, A. (1975) Crystal-chemical interpretation of crystallographic anomalies in lunar plagioclase. *Bulletin de la Société Française de Minéralogie et de Crystallographie*, 98, 113–117.
- Burke, J. (1965) *The Kinetics of Phase Transformation in Metals*. Pergamon Press Ltd.
- Burton, J. A., Prim, R. C., and Slichter, W. P. (1953) The distribution of solute in crystals grown from the melt. *Journal of Chemical Physics*, 21, 1987–1989.
- Donaldson, C. H., Usselman, T. M., Williams, R. J., and Lofgren, G. E. (1975) Experimental modeling of the cooling history of Apollo 12 olivine basalts. *Proceedings of the Lunar Science Conference 6th*, 843–869.
- Dowty, E. (1976) Crystal structure and crystal growth: II. Sector zoning in minerals. *American Mineralogist*, 61, 460–469.
- Dowty, E. (1980) Crystal growth and nucleation theory and the numerical simulation of igneous crystallization. In R. B. Hargraves, Ed., *Physics of Magmatic Processes*, p. 419–485. Princeton Univ. Press, Princeton.
- Freer, R., Carpenter, M. A., Long, J. V. P., and Reed, S. J. B. (1982) "Null result" diffusion experiments with diopside: Implications for pyroxene equilibria. *Earth and Planetary Science Letters*, 58, 285–292.
- Gamble, R. P. and Taylor, L. A. (1980) Crystal liquid partitioning in augite: Effect of cooling rate. *Earth and Planetary Science Letters*, 47, 21–33.
- Grove, T. L. and Bence, A. E. (1977) Experimental study of pyroxene-liquid interaction in quartz-normative basalt 15597. *Proceedings of the Lunar Science Conference 8th*, 1549–1579.
- Grove, T. L. and Walker, D. (1977) Cooling histories of Apollo 15 quartz normative basalts. *Proceedings of the Lunar Science Conference 8th*, 1501–1520.
- Grove, T. L. and Raudsepp, M. (1978) Effects of kinetics on the crystallization of quartz normative basalt 15597: An experimental study. *Proceedings of the Lunar and Planetary Science Conference 9th*, 585–599.
- Grove, T. L. and Bence, A. E. (1979) Crystallization kinetics in a multiply saturated basalt magma: An experimental study of Luna 24 ferrobasalt. *Proceedings of the Lunar and Planetary Science Conference 10th*, 439–478.
- Hopper, R. W. and Uhlmann, D. R. (1974) Solute redistribution during crystallization at constant velocity and constant temperature. *Journal of Crystal Growth*, 21, 203–213.
- Huebner, J. S. and Turnock, A. C. (1980) The melting relations at 1 bar of pyroxenes composed largely of Ca-, Mg-, and Fe-bearing components. *American Mineralogist*, 65, 225–271.
- Kern, R. (1953) Etude du facies de quelques cristaux ioniques a structure simple. *Bulletin de la Société Française de Minéralogie et de Crystallographie*, 76, 325–391.
- Kirkpatrick, R. J. (1981) Kinetics of crystallization of igneous rocks. In A. C. Lasaga and R. J. Kirkpatrick, Ed., *Kinetics of Geological Processes*, p. 321–398. Mineralogical Society of America, Washington.
- Kirkpatrick, R. J., Kuo, L. C., and Melchior, J. (1981) Crystal growth in incongruently-melting compositions: programmed cooling experiments with diopside. *American Mineralogist*, 66, 223–241.
- Kitamura, M. and Sunagawa, I. (1977) The effective distribution of solute and the anisotropy of a crystal. *International Conference of Crystal Growth*, Collected Abstracts, 5, 91.
- Klein, L. and Uhlmann, D. R. (1974) Crystallization behaviour of anorthite. *Journal of Geophysical Research*, 79, 4869–4874.
- Kouchi, A., Sugawara, Y., Kashima, K., and Sunagawa, I. (1983a) Laboratory growth of sector zoned clinopyroxenes in the system  $\text{CaMgSi}_2\text{O}_6\text{-CaTiAl}_2\text{O}_6$ . *Contributions to Mineralogy and Petrology*, 83, 177–184.
- Kouchi, A., Hosoya, S., Kitamura, M., Takei, H., and Sunagawa, I. (1983b) The effects of crystallographic orientation, interface type and growth kinetics on Ni distribution between olivine and its melt. *Physics and Chemistry of Mineralogy*, 9, 167–172.
- Lindstrom, D. J. (1983) Kinetic effects on trace element partitioning. *Geochimica et Cosmochimica Acta*, 47, 617–622.
- Lofgren, G. E. (1974) Temperature induced zoning in synthetic plagioclase feldspar. In W. S. Mackenzie and J. Zussmann, Ed., *The Feldspar*, p. 362–375. Manchester Univ. Press, Manchester.
- Lofgren, G. E. (1980) Experimental studies on the dynamic crystallization of silicate melts. In R. B. Hargraves, Ed., *Physics of Magmatic Processes*, p. 487–551. Princeton Univ. Press, Princeton.
- Longhi, J., Walker, D., and Hays, J. F. (1976) Fe and Mg in plagioclase. *Proceedings of the Lunar Science Conference 7th*, 1281–1300.
- Loomis, T. P. (1981) An investigation of disequilibrium growth processes of plagioclase in the system anorthite-albite-water by methods of numerical simulation. *Contributions to Mineralogy and Petrology*, 76, 196–205.
- Loomis, T. P. (1982) Numerical simulations of crystallization processes of plagioclase in complex melts: The origin of major and oscillatory zoning in plagioclase. *Contributions to Mineralogy and Petrology*, 81, 219–229.
- Nakamura, Y. (1973) Origin of sector-zoning of igneous clinopyroxenes. *American Mineralogist*, 58, 986–990.
- Nakamura, Y. and Kushiro, I. (1970) Compositional relation of coexisting orthopyroxene, pigeonite and augite in a tholeiitic andesite from Hakone Volcano. *Contributions to Mineralogy and Petrology*, 26, 265–275.
- Smith, J. V. (1974) *Feldspar Minerals*, vol. 2, p. 686. Springer-Verlag, New York, Heidelberg, Berlin.
- Smith, R. K. and Lofgren, G. E. (1983) An analytical and experimental study of zoning in plagioclase. *Lithos*, 16, 153–168.
- Tarshis, L. A. and Tiller, W. A. (1967) The effect of interface kinetics on the morphological stability of a planar interface during solidification. In H. S. Peiser Ed., p. 709–719. Oxford Pergamon.
- Tsuchiyama, A. (1983) Crystallization kinetics in the system  $\text{CaMgSi}_2\text{O}_6\text{-CaAl}_2\text{Si}_2\text{O}_8$ : the delay in nucleation of diopside and anorthite. *American Mineralogist*, 68, 687–698.
- Tsuchiyama, A. and Takahashi, E. (1983) Melting kinetics of a plagioclase feldspar. *Contributions to Mineralogy and Petrology*, 84, 345–354.
- Tsuchiyama, A., Nagahara, H., and Kushiro, I. (1980) Experimental reproduction of textures of chondrules. *Earth and Planetary Science Letters*, 48, 155–165.
- Tsuchiyama, A., Kitamura, M., and Sunagawa, I. (1981) Distri-

- bution of elements in growth of (Ba, Pb)  $(\text{NO}_3)_2$  crystals from aqueous solution. *Journal of Crystal Growth*, 55, 510-516.
- Usselman, T. M., Lofgren, G. E., Donaldson, C. H., and Williams, R. J. (1975) Experimentally reproduced textures and mineral chemistries of high-titanium mare basalts. *Proceedings of the Lunar Science Conference 6th*, 997-1020.
- Walker, D., Kirkpatrick, R. J., Longhi, J., and Hays, J. F. (1976) Crystallization history of lunar picritic basalt sample 12002: Phase equilibria and cooling-rate studies. *Geological Society of America Bulletin*, 87, 646-656.
- Walker, D., Powell, M. A., Lofgren, G. E., and Hays, J. F. (1978) Dynamic crystallization of a eucrite basalt. *Proceedings of the Lunar and Planetary Science Conference 9th*, 1369-1391.
- Yoder, H. S. Jr. (1976) Generation of basaltic magma. *National Academy of Science, Washington D. C.*

*Manuscript received, May 4, 1984;  
accepted for publication, January 3, 1985.*